Low operating temperature CO sensor prepared using SnO₂ nanoparticles

I-Chen Lin, Chung-Chieh Chang, Chung-Kwei Lin, Shao-Ju Shih, Chi-Jung Chang, Chien-Yie Tsay, Jen-Bin Shi, Tzyy-Leng Horng, et al.

ONLINE FIRST

JECR | Journal of Electroceramics

Volume 22 · Number 1 · February 2014

Springer

CrossMark

Low operating temperature CO sensor prepared using SnO$_2$ nanoparticles

I-Chen Lin[1] · Chung-Chieh Chang[2] · Chung-Kwei Lin[2] · Shao-Ju Shih[3] · Chi-Jung Chang[4] · Chien-Yie Tsay[1] ·
Jen-Bin Shi[5] · Tzyy-Leng Horng[6] · Jing-Heng Chen[7] · Jerry J. Wu[8] · Ching-Ying Hung[1] · Chin-Yi Chen[1]

Abstract

A low operating temperature CO (carbon monoxide) sensor was fabricated from a nanometer-scale SnO$_2$ (tin oxide) powder. The SnO$_2$ nanoparticles in a size range 10–20 nm were synthesized as a function of surfactant (tri-n-octylamine, TOA) addition (0–1.5 mol%) via a simple thermal decomposition method. The resulting SnO$_2$ nanoparticles were first screen-printed onto an electrode patterned substrate to be a thick film. Subsequently, the composite film was heat-treated to be a device for sensing CO gas. The thermal decomposed powders were characterized by field-emission scanning electron microscopy (FESEM), X-ray diffractometry (XRD), and surface area measurements (BET). The CO-sensing performance of all the sensors was investigated. The experimental results showed that the TOA addition significantly decreased the particle size of the resulting SnO$_2$ nanoparticle. However, the structure of the powder coating was crucial to their sensing performance. After heat-treatment, the smaller particle tended to cause the formation of agglomeration, resulting in the decline of surface area and reducing the reaction site during sensing. However, the paths for the sensed gas entering between the agglomerated structure may influence the sensing performance. As a CO sensing material, the SnO$_2$ nanoparticle (~12 nm in diameter) prepared with 1.25 mol% TOA addition exhibited most stable electrical performance. The SnO$_2$ coating with TOA addition >0.75 mol% exhibited sensor response at a relatively low temperature of <50°C.

Keywords SnO$_2$ · CO sensor · Low temperature · Thermal decomposition · Sensor response

1 Introduction

Exhaust gas emitted from industrial plants and vehicles increases tremendously with increasing the rate of the advances in industrial technology and accelerations in economic development. The corresponding standards for gas emissions of SO$_2$, NOx, CO$_2$, CO, O$_3$ etc. are thus regulated by government agencies to meet the demanding environmental criteria.

The carbon monoxide is an odorless, colorless, tasteless, but poisonous gas, being able to exist in atmosphere to cause death as well as serious long term health problem such as brain damage. Such highly toxic gas is mainly produced from the exhaust of internal combustion engines and the incomplete burning of gas, liquid petroleum gas (LPG), fossil fuels as well as solid fuels such as coal, wood, and some organic matters. Because the carbon monoxide poisoning may result in headache, nausea, vomiting, coma, and even fatality, the

✉ Chin-Yi Chen
chencyi@fcu.edu.tw

1 Department of Materials Science and Engineering, Feng Chia University, Taichung 407, Taiwan

2 School of Dental Technology, College of Oral Medicine, Taipei Medical University, Taipei 110, Taiwan

3 Department of Materials Science and Engineering, National Taiwan University of Science and Technology, Taipei 106, Taiwan

4 Department of Chemical Engineering, Feng Chia University, Taichung 407, Taiwan

5 Department of Electronic Engineering, Feng Chia University, Taichung 407, Taiwan

6 Department of Applied Mathematics, Feng Chia University, Taichung 407, Taiwan

7 Department of Photonics, Feng Chia University, Taichung 407, Taiwan

8 Department of Environmental Engineering and Science, Feng Chia University, Taichung 407, Taiwan

⌂ Springer

detection and monitoring of the concentration of carbon monoxide is crucial for the poisoning prevention [1].

Gas sensor which is composed of nanostructured oxide semiconductor with extremely high specific surface area possesses competitive advantages for achieving a high sensitivity and rapid response [2], due to the high sensing reaction involving redox interaction between the target gas and the charged oxygen adsorbed on the surface. Generally, zinc oxide (ZnO) [3], titanium oxide (TiO$_2$) [4], cerium oxide (CeO$_2$) [5] and tin oxide (SnO$_2$) [6–8] have been widely studied for the application of gas sensors [1]. In the literature, SnO$_2$ with nanostructures such as nanoparticle [9], nanotube [10], nanorod [11], nanowire [12] and nanosheet [2] has attracted much attention and been intensely reported. However, the operating temperature for most metal oxide gas sensor is in a range from 300 to 500 °C [13]. At high temperatures, small grains tend to form into large agglomerates, decreasing both surface areas and catalytic properties of the material [14]. Moreover, low power consumption issue and the use for heat resistant materials around the sensor coatings become very important for the durability of the sensor device [13, 15]. Therefore, reductions in operating temperature of the sensing materials is one of the directions that numerous researchers are keen to find out recently.

Though several studies have demonstrated that the operating temperature of SnO$_2$ powder coatings can be lowered by either doping with noble metals [16–18] or being deposited onto various nanostructures [19, 20] for the applications of gas sensors; to the best of our knowledge, the undoped SnO$_2$ nanoparticle has not yet been coated directly to optimize systematically the low-temperature CO sensing performance by powder synthesis. In this study, undoped nanosize SnO$_2$ powders were synthesized as a function of TOA surfactant addition by thermal decomposition method; subsequently, the powders were screen-printed onto a Pt-electrode coated Al$_2$O$_3$ substrate for the fabrication of a CO sensor. Post heat treatments were carried out to improve the thermal stability of the SnO$_2$ nanoparticle coating before the sensing properties were measured. The particulate morphology of the resulting powders was observed by high resolution transmission electron microscopy (HRTEM). The phase and microstructure of the nanoparticle films were identified by X-ray diffractometry (XRD) and scanning electron microscopy (SEM), respectively. The electrical resistive behavior of the SnO$_2$ coatings was measured under various CO concentrations as a function of operating temperature. The sensing behavior, including the sensor response of the powder coatings to changes in CO concentrations, was investigated as a function of TOA addition.
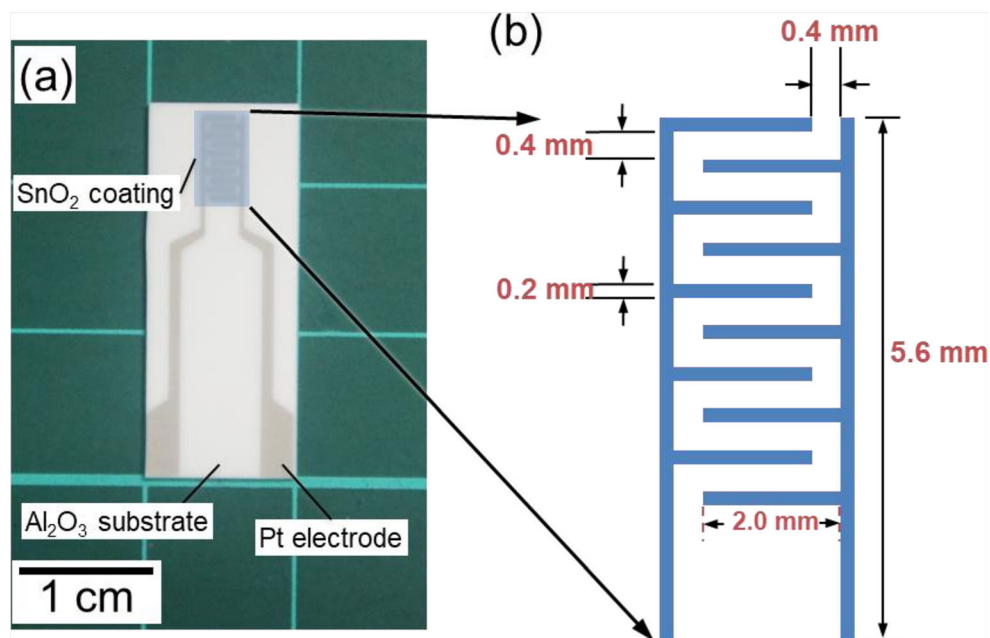
2 Experimental procedures

In the present study, the CO sensing properties of a SnO$_2$ coating were investigated by screen printing SnO$_2$ powders onto alumina substrate. The SnO$_2$ powders were synthesized from the thermal decomposition of tin (II) chloride dihydrate (TCD) in oleic acid (OA) as a function of tri-n-octylamine (TOA) concentration. The chemical formulas of TCD, OA and TOA are SnCl$_2$·2H$_2$O (Sigma-Aldrich, Inc., USA), C$_{18}$H$_{34}$O$_2$ (Aldrich Chem. Co., Inc., USA) and C$_{24}$H$_{51}$N (Alfa Aesar, A Johnson Matthey Co., USA), respectively, being the precursor, solvent and surfactant in the thermal decomposition process. They are all at reagent grades. The respective molecular weights of TCD, OA and TOA reported by the manufacturers are 225.65, 282.47 and 353.67. The concentrations of TOA were set at 0, 0.75, 1.00, 1.25 and 1.50 mol%. The metal salt dissolved precursor solution with various surfactant additions was stirred and heated up to a temperature of 200°C for 1 h for removal of the hydration water; then, the solution was further heated to a temperature of 310°C for thermal decomposition reaction for 1 h. After cooling to room temperature, the precipitates were rinsed by n-hexane and ethanol repetitively. After centrifuging and drying, the SnO$_2$ powders were obtained by heat-treatment at 500°C for 2 h.

Subsequently, the resulting powders were mixed with organics to produce a paste for screen printing onto a Pt-electrode-printed alumina substrate (10 mm × 25 mm × 0.6 mm). Detailed compositions of the coating paste can be found elsewhere [21, 22]. Single interdigital structure of Pt electrode was designed for sensing measurements. The details of the interdigital electrode configuration are presented in Fig. 1. To remove the residual organics and confirm the formation of the oxide coating, the screen-printed thick films were heat-treated at 500 °C for 5 h in air (TF55035A, Lindberg/Blue M, USA). The heating and cooling rates were 5 °C/min. Subsequently, the CO sensing properties of the powder coatings were characterized.

The microstructures of as-prepared powders and heat-treated thick films were observed using high resolution transmission electron microscopy (TEM, 1200EX, JEOL II, Japan) and field emission scanning electronic microscopy (FE-SEM, Hitachi S-4800, Japan), respectively. The phases were identified by X-ray diffractometry using Cu$K\alpha$ radiation (XRD, SRA M18XHF, MacScience Co., Ltd., Japan). The specific surface areas of the powders were determined by BET (Brunauer-Emmer-Teller) method from nitrogen adsorption and desorption isotherm data obtained at −196 °C on a constant-volume adsorption apparatus (SA-9600 Series, HORIBA, Japan). The electrical resistance of the thick films was recorded in a homemade chamber (9.5-cm inner diameter, 12.2-cm height) as a function of temperature upon exposure to various concentrations of CO gas by a data acquisition apparatus (Agilent 34970A, USA). The sensor was back-heated by a Pt-electrode-printed Al$_2$O$_3$ substrate which was connected to a DC power supply (Motech DR 2004, Taiwan) for the temperature/voltage controller. In the test of the CO sensor, the output resistances were recorded as a function of

Fig. 1 Interdigital structure electrodes used for sensor characterizations of (**a**) Pt-electrode printed Al_2O_3 substrate in the present study. The details of the interdigital electrode configuration are also schematically drawn in figure (**b**)

temperature in the CO concentration range of 100–800 ppm. The sensors were kept at least for 20 min at each temperature to reach equilibrium before any CO exposure. The sensor response of CO was defined as the ratio of R_{air}/R_{gas}, where R_{air} is the average sensor resistance in clean air and R_{gas} is the average sensor resistance during CO exposure once the response has stabilized.

3 Results and discussion

SnO_2 powders synthesized as a function of surfactant (TOA) concentration by thermal decomposition were coated on substrate for use in the CO sensor in the present study. Figure 2 shows the XRD patterns of the as-prepared SnO_2 powders after thermal decomposition as a function of TOA concentration. The powder mixtures were identified as a tetragonal SnO_2 phase by the diffraction peaks, in accordance with JCPDS file No. 41–1445. No peaks but those of SnO_2 were observed. The broadened peaks indicated that the powders were nanocrystalline. The crystallite sizes for the TOA concentration at 0, 0.75, 1.00, 1.25, and 1.5 mol% were respectively calculated to be ca. 40, 22, 11, 12, and 26 nm by Scherrer's formula, as shown in Table 1. An obvious decrease in crystallite size was found when a small amount of TOA surfactant was added, then the crystallite size increased with the increase in added TOA concentration. This suggested that a relatively small crystallite size of the thermal decomposed SnO_2 can be obtained when an appropriate amount of surfactant was used. A likely explanation for the smaller particle size is that trioctylamine can act as capping agents for the preferential growth in specific direction for nanomaterials [23].

Therefore, the presence of the TOA may act as a capping agent (stabilizer) which bound to a face changed the free energy of that face and hence slowed the growth rate of SnO_2 crystallite.

Figure 3 shows the SEM micrographs of the as-prepared SnO_2 powders as a function of TOA concentration. Note that the size of the particles first decreased with the increase of surfactant concentration, then increased when the surfactant concentration increased. The diameters of the SnO_2 particle (in Fig. 3(a)-(e)) for the added TOA concentrations at 0, 0.75, 1.00, 1.25, and 1.5 mol% were ca. 40, 20, 10, 10 and 25 nm, respectively. The particle sizes were very close to the
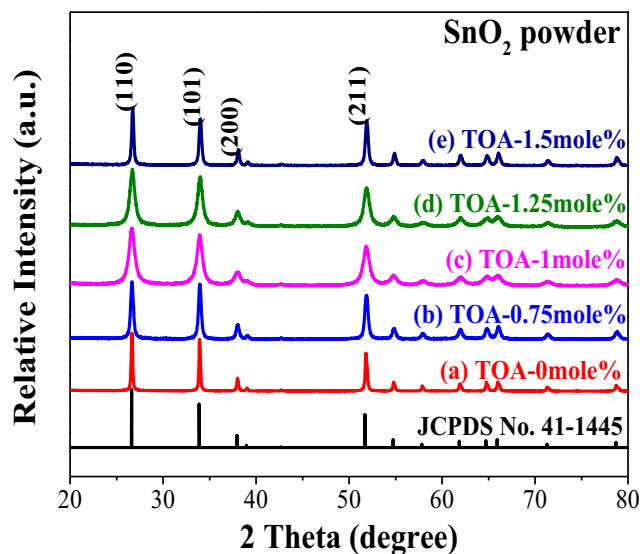

Fig. 2 XRD patterns of as-precipitated powders with (**a**) unadded, (**b**) 0.75, (**c**) 1.00, (**d**) 1.25, and (**e**) 1.50 mol% TOA surfactant. The corresponded JCPDS pattern for SnO_2 is also presented for comparison

Table 1 Crystallite size, particle size and BET surface area of the SnO$_2$ powders as a function of TOA surfactant concentration

SnO$_2$ powder-TOA surfactant concentration (mol%)	Crystallite size (nm) determined by XRD	particle size (nm) determined by SEM	BET surface area (m^2/g)
SnO-0	40 ± 4.75	40 ± 5.4	5.60
SnO-0.75	22 ± 0.97	20 ± 2.0	8.25
SnO-1.00	11 ± 0.61	10 ± 1.2	27.37
SnO-1.25	12 ± 0.50	10 ± 1.8	8.81
SnO-1.50	26 ± 2.43	25 ± 3.9	7.76

crystallite sizes calculated from XRD patterns, suggesting each SnO$_2$ particle was made up of single crystallite. The smallest particle size of thermal decomposed SnO$_2$ was estimated to be ca. 10 nm at TOA concentrations of 1.00 and 1.25 mol%. Some agglomerates with an irregular morphology can be observed in the coating structures. Severer nanoparticle agglomeration occurred when particle size was smaller than 20 nm (Fig. 3(c) and (d)). Generally, the smaller the particle

size of gas-sensing material, the higher the sensor performance obtained. Microstructure of as-prepared SnO$_2$ nanoparticles was further studied in detail with the observation of transmission electron microscopy. Figure 4 shows the TEM, HRTEM images and SAED (selected area electron diffraction) pattern of the thermal decomposed SnO$_2$ powder as TOA concentration was 1.25 mol%. From the bright field image (Fig. 4(a)), the SnO$_2$ powder was composed of clustered nanometric particles, revealing a rounded shape with a mean diameter of about 15 ± 5 nm. As seen in HRTEM image (Fig. 4(b)), the presence of Moiré fringes well confirmed the crystalline nature and single crystallite of each SnO$_2$ nanoparticle as mentioned above. Inter planner spacing (2.3 Å) estimated experimentally is in good agreement with that expected for (200) plane of tetragonal phase of SnO$_2$. SAED pattern (Fig. 4(c)) shows a set of four dashed circular rings obtained due to diffraction of electrons from indexed (110), (101), (200) and (211) planes of tetragonal SnO$_2$. Furthermore, Table 1 also shows BET surface area of the SnO$_2$ powders as a function of TOA concentration. The surface areas were 5.6, 8.25, 27.37, 8.81 and 7.76 m^2/g for the thermal decomposed SnO$_2$ powders when TOA surfactant

Fig. 3 SEM micrographs of as-prepared SnO$_2$ powders with (**a**) unadded, (**b**) 0.75, (**c**) 1.00, (**d**) 1.25, and (**e**) 1.50 mol% TOA surfactant. Low-magnification SEM images of the powders (**a–e**) are also inset in their corresponding micrographs
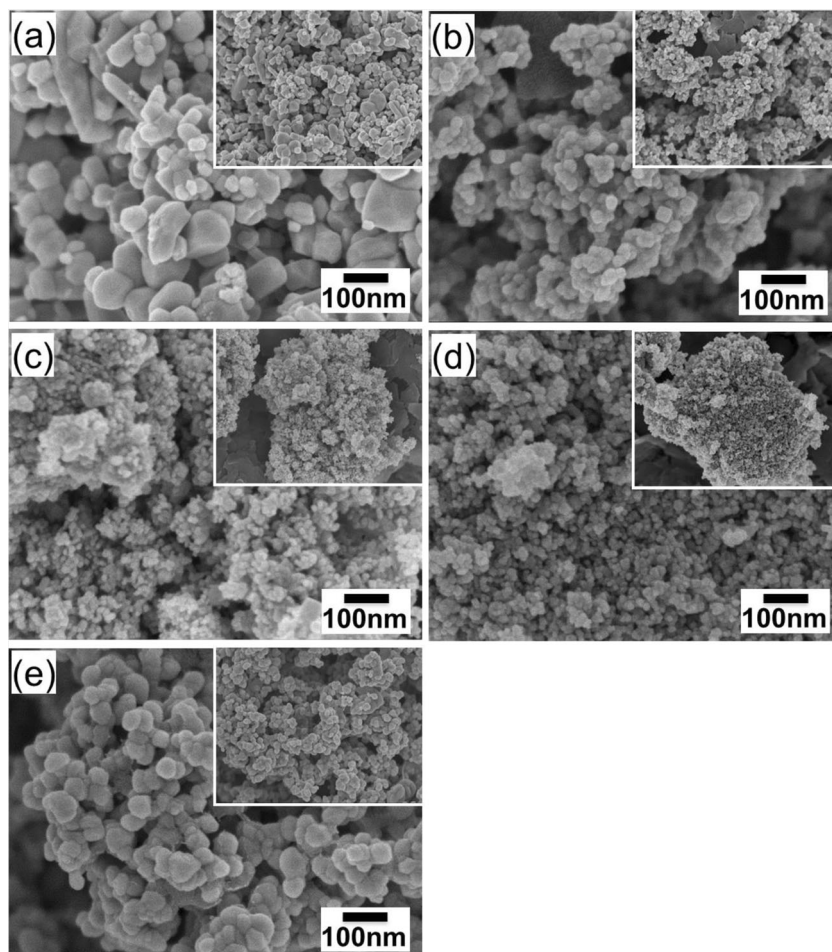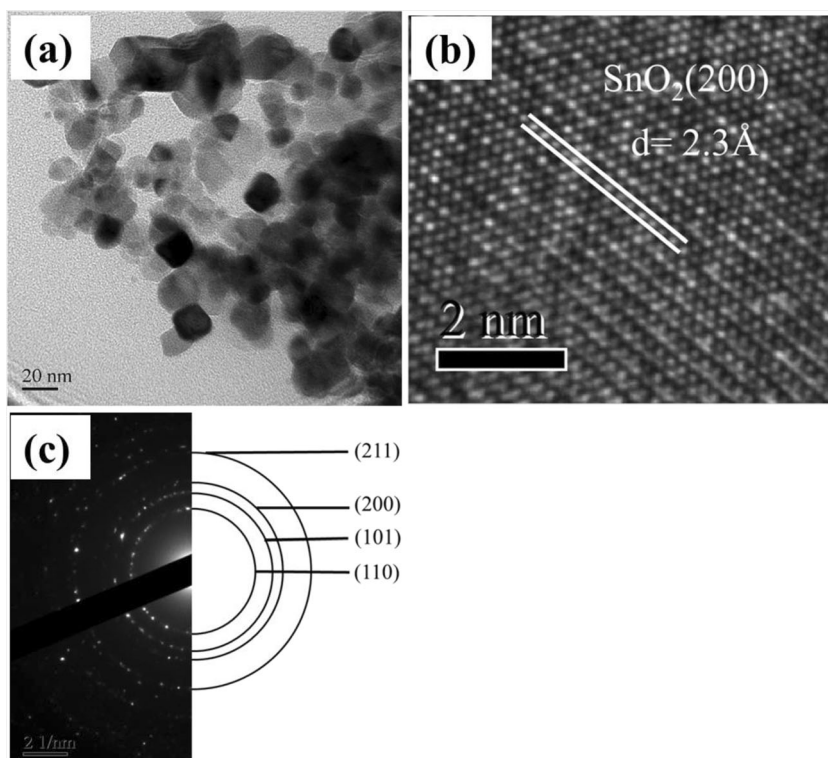
Fig. 4 (**a**) TEM, (**b**) HRTEM images and (**c**) SAED patterns of thermal decomposed SnO_2 powder by adding 1.25 mol% surfactant TOA
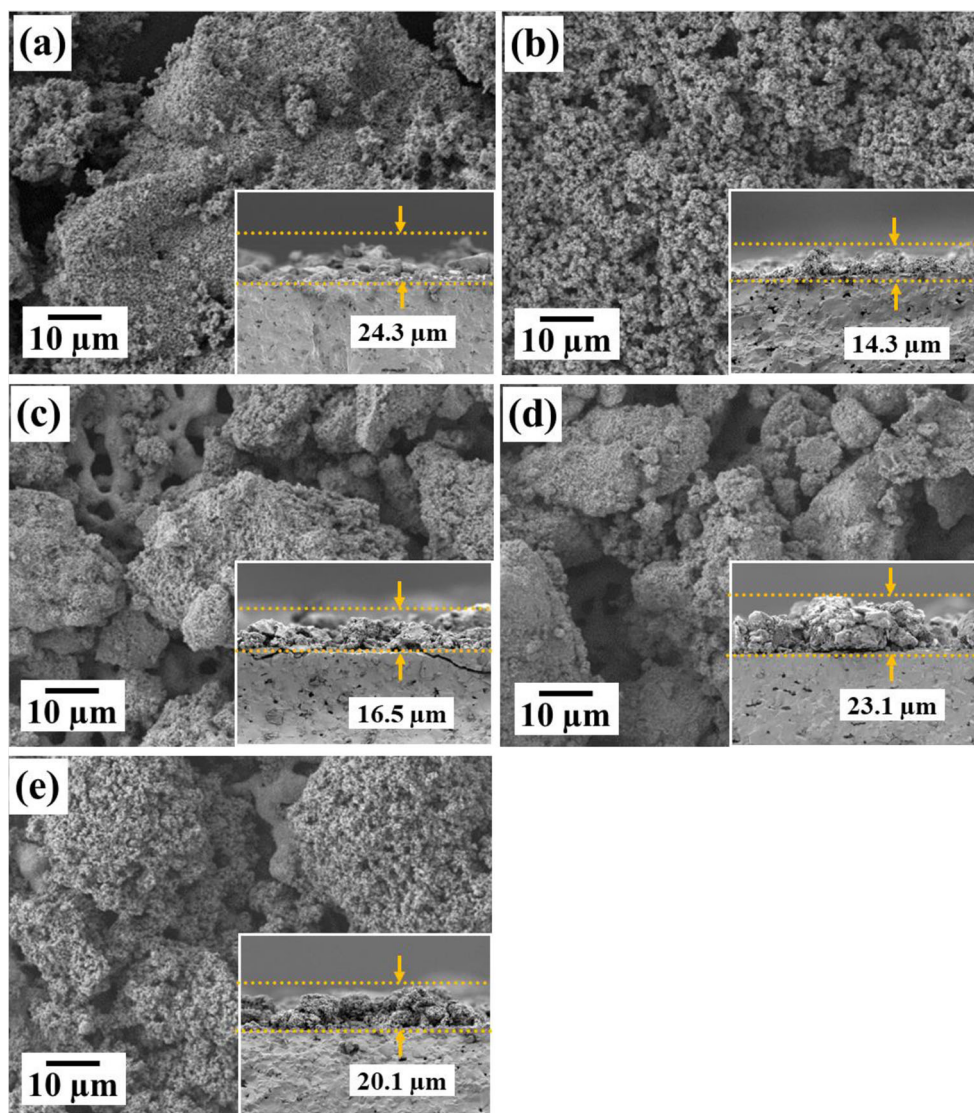

concentrations were 0, 0.75, 1.00, 1.25 and 1.50 mol%, respectively. In comparison to the crystallite size, it is reasonable that the smallest crystallite size exhibited the highest surface area. Theoretically, sensor material with higher surface area provides a larger amount of available active sites for sensing target gases, a better sensing performance of such powder coating may thus be expected.

From the SEM and TEM estimation, the SnO_2 coatings with a particle size of ca. 10–20 nm were thus expected to exhibit relatively good sensor performance. Similar trend can be found in the crystallite size of SnO_2 powders estimated by XRD. Therefore, the microstructural results suggested that one SnO_2 particle was per one crystallite in the present system. Subsequently, the powders were applied onto the electrode-printed substrates by screen printing. After heat-treatment, Fig. 5 shows the top-view SEM micrographs of the as-heated SnO_2 coatings as a function of TOA concentration. The morphology of SnO_2 coating was uniform but loose as TOA addition was 0.75 mol%. Instead, heat-treated agglomeration tended to become significant when the initial particle size was fine. Island-like morphology was thus found in the coatings when TOA concentrations were higher than 0.75 mol%. In some cases, however, island-like coating with well connecting structures exhibits better sensing performances [22]. The side-view SEM micrographs were also shown in the insets in their corresponding images. The thicknesses of coatings can thus be confirmed by the side-view images. Note that the thicknesses of the SnO_2 coatings for TOA concentrations of 0.75, 1.00, 1.25, and 1.5 mol% were

14.3, 16.5, 23.1 and 20.1 μm, respectively. The average thickness was 18.5 ± 3.4 μm.

Figure 6 shows the sensor response, R_{air}/R_{gas}, of the SnO_2 powder coatings with various TOA additions under different CO concentrations as a function of sensing temperature. Since the coating of the SnO_2 powder without TOA addition was discontinuous, showing no sensing behavior in this system, the sensor performances of the coating without TOA addition are not discussing in the follow-up experimental results. Note in Fig. 6(a) that the sensor response of the coatings can only be observed in a higher temperature range $\geq 250°C$ when 0.75 mol% TOA surfactant was used. However, in Fig. 6(b)-(d), the SnO_2 coating with larger than 0.75 mol% TOA addition exhibited sensor response in a relatively low temperature range $(< 50°C)$. The powder coating with 1.25 and 1.50 mol% TOA addition showed higher sensor response in this system, as shown in Fig. 6(c) and (d). Moreover, the sensor response tended to increase with the increase in sensing CO concentration. Similar trend can generally be found in earlier reported works [13, 14, 24] when sensing temperature is below 300°C. Note that the sensor response ranged from ca 0.75 to 2.25 at operating temperatures of 25–300°C, as seen in Fig. 6(b)-(d). Though such values were not as high as those reported in the literature [13, 24], they are still comparable with those reported by some works [2, 25–27]. This is most likely attributed to the influence of the microstructure, porosity as well as thickness of the powder coating [2, 24, 28]. The particle size of SnO_2 powders showed no obvious and direct influences on the sensor response in this system. Instead, the

Fig. 5 Top-view SEM micrographs of as-heated SnO$_2$ powders with (**a**) unadded, (**b**) 0.75, (**c**) 1.00, (**d**) 1.25, and (**e**) 1.50 mol% TOA surfactant. Side-view SEM micrographs of the powder coatings (**a–e**) are also inset in their corresponding micrographs
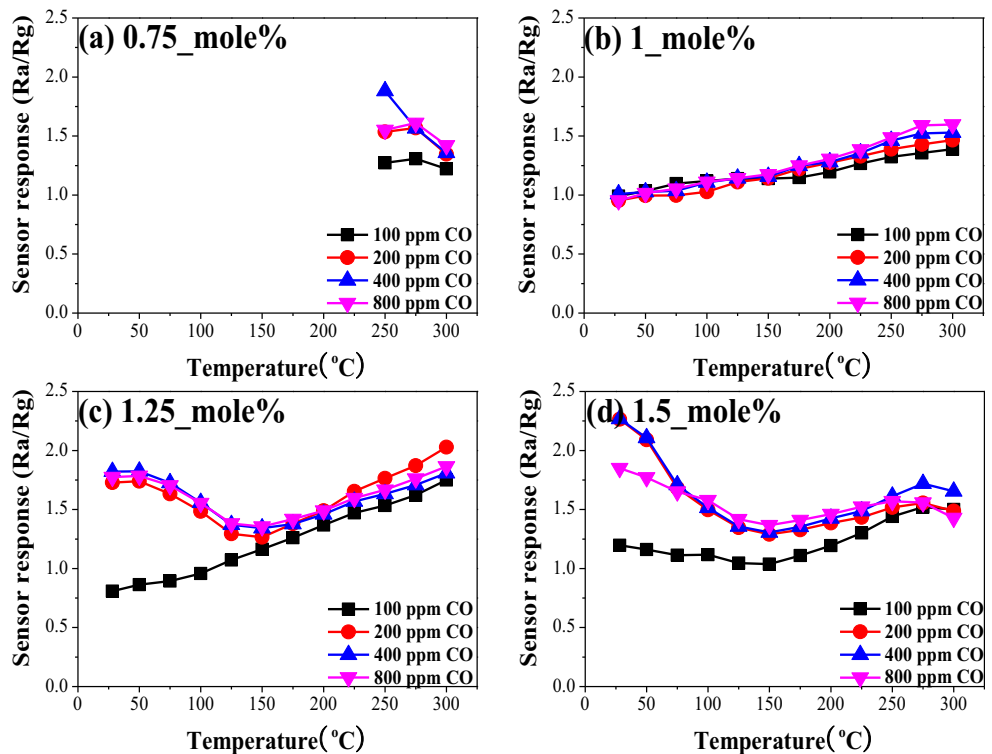

structure of the powder coating that may be influenced by the particle size was thought to be crucial to their sensing performance.

Figure 7 shows the sensor response of the SnO$_2$ powder coatings under different CO concentrations at various sensing temperatures as a function of surfactant TOA additions. Note that the SnO$_2$ coatings exhibited higher response at a sensing temperature of 300 °C when TOA concentration was low ($\leq$ 1.25 mol%). As mentioned above, Fig. 7(a)-(d), the sensor response increased with the increase in TOA surfactant concentration as sensing temperature below 300 °C. Under all the concentrations of CO gas, the SnO$_2$ coatings exhibited sensor response at a relatively low temperature of 25 °C when TOA addition higher than 1.00 mol%. The powder coating with 1.50 mol% TOA addition possessed highest sensor response at 25 °C when CO concentration was $\geq$200 ppm in this system. Moreover, Fig. 8 shows the corresponding dynamic sensor response of SnO$_2$ coating with 1.25 mol% TOA addition

as a function of time toward the change in CO concentration at 50 °C. Note that the SnO$_2$ coating showed almost no response toward a change in CO concentration in the range of air to 100 ppm, and exhibited a sensing behavior when the CO concentration was higher than 200 ppm. The response tended to increase with the increase in sensing CO concentration, showing a reasonable trend comparing to that at 300 °C [29]. When the CO atmosphere returned to air, the resistance of SnO$_2$ coating also recovered. However, the sensing mechanism of the SnO$_2$ coating at low temperature is not thought to be totally similar to that at 300 °C in this system. This was generally believed to be additionally interfered by the humidity [14]. Further investigations are thus still required to clarify the mechanism(s).

Figure 9 shows the resistance and sensor response of SnO$_2$ coatings using various TOA additions as a function of CO concentration at a sensing temperature of 50 °C. The resistance of SnO$_2$ coating with 0.75 mol% TOA addition was not
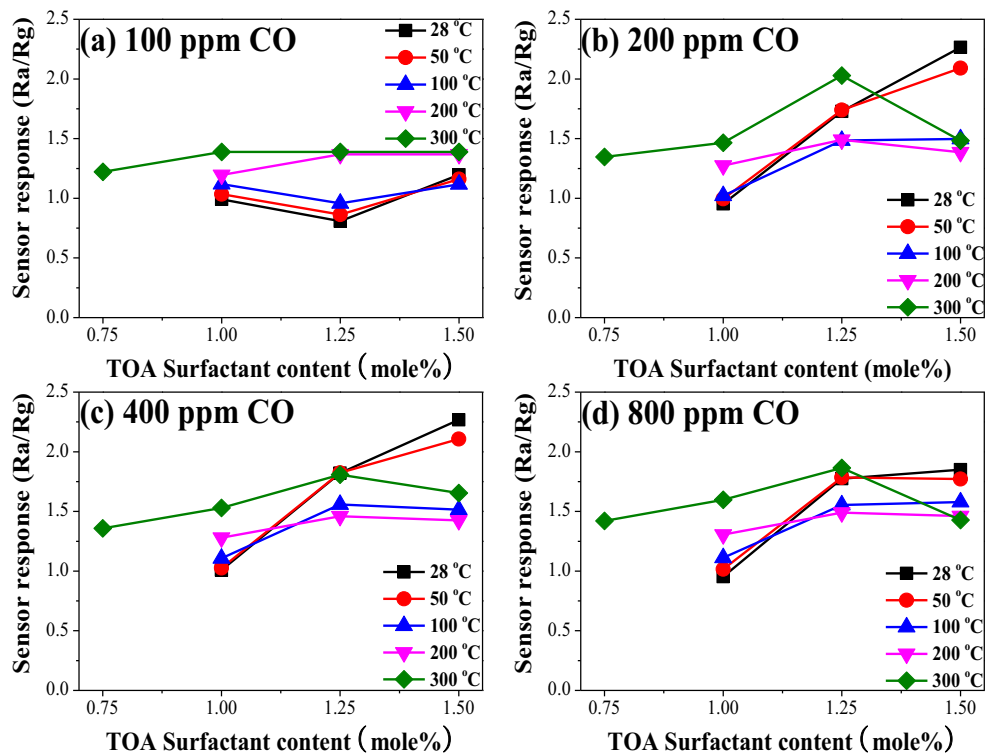
J Electroceram

Fig. 6 Sensor response of SnO₂ powder coatings with (**a**) 0.75, (**b**) 1.00, (**c**) 1.25, and (**d**) 1.50 mol% TOA additions under different CO concentrations as a function of sensing temperature

shown for comparison in these figures because its resistance value was higher than the limitation ($1.2 \times 10^8 \ \Omega$) of the instrument. Note in Fig. 9(a) that the resistance of the coatings decreased with the increase of the TOA surfactant addition when sensing temperature was at 50°C. Except the resistance

of the coating with 1.0 mol% TOA addition, the measurable resistance decreased as the sensing CO concentration increased. According to the difference in resistance between the coatings under CO and air, the SnO₂ powder coating with 1.5 mol% TOA addition exhibited better sensing behavior,

Fig. 7 Sensor response of SnO₂ powder coatings at different sensing temperatures as a function of TOA addition under CO concentrations of (**a**) 100 ppm, (**b**) 200 ppm, (**c**) 400 ppm, and (**d**) 800 ppm
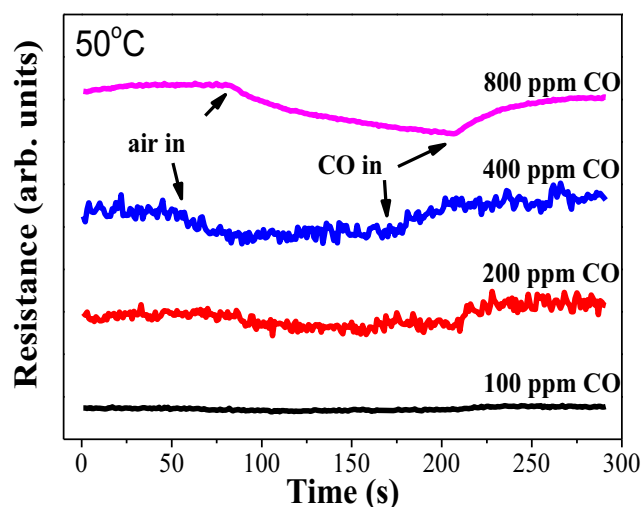
Fig. 8 Dynamic sensor response of SnO$_2$ powder coating with 1.25 mol% TOA addition as a function of time toward the change in CO concentration at 50 °C

showing a decreasing trend when the CO concentration was higher than 100 ppm.

To understand the ratio of resistance changes when the coatings encounter the change in concentration of the sensing gas, the resistances were converted as a function of CO concentration into the sensor response, as shown in Fig. 9(b). Generally, powders with fine particle sizes, narrow particle size distributions and extremely high surface area tend to result in severe agglomeration, see the data of SnO$_2$ particle with 1.00 mol% TOA addition in Table 1, causing the low connectivity of the sensing particles after heat treatment. The decrease in resistance was insusceptible when the CO concentration increased, as shown in Fig. 9(a). The SnO$_2$ powder coating with 1.00 mol% TOA addition thus exhibited no significant sensor response toward the change in CO concentration. The sensor response of the coatings with 1.25 and 1.50 mol% TOA additions increased when the CO concentration increased from 100 ppm to 200 ppm, and then remained constant at ~2 when the CO concentration further increased.
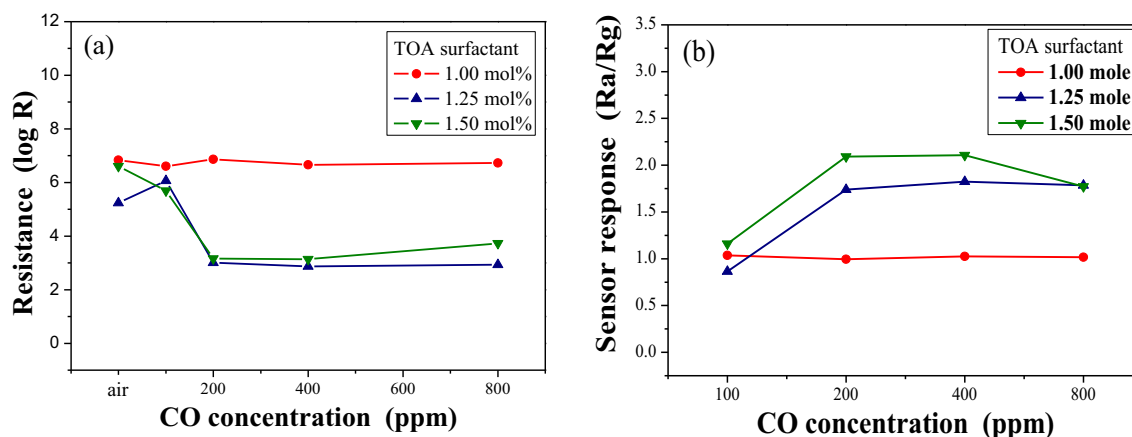
The SnO$_2$ coating with 1.50 mol% TOA addition (the powder sample with lower surface area) exhibited highest sensor response of 2.1 toward a CO concentration of 200 ppm at 50 °C. Recall the statement mentioned above, sensor material with higher surface area may provide a large amount of available active sites to show a better sensing performance. This was most likely attributed to the gaps between the island-like structure may provide paths for the sensed gas to enter the coating structure. Because the crystallinity seemed not influence the fact that gas sensing with nanostructures can work at low temperatures [30], the sensor response of metal-oxide gas sensors depends on their microstructures of the sensing materials such as particle size [28], porosity, connectivity [22], etc. Such structure with an acceptable connectivity thus exhibited better sensing properties in this system.

4 Conclusions

The structure of a SnO$_2$ coating dominates its CO gas sensing properties. SnO$_2$ powders were prepared by thermal decomposition methods as a function of TOA surfactant addition, and screen printed onto Al$_2$O$_3$ substrates for investigation of their CO sensor properties. The resulting powders were identified as a tetragonal SnO$_2$ phase and observed to have a relatively small particle size ranging in ca. 10–40 nm. After heat treatment, the SnO$_2$ powder coatings transformed from a uniformly loose structure to an island-like structure with increases in the TOA surfactant addition. The paths between the island-like structures for the sensed gas entering the coating became significantly influencing the sensing performance. The SnO$_2$ coating with higher than 0.75 mol% TOA addition can show comparable sensor response at a relatively low temperature < 50°C. Toward all the concentrations (100–800 ppm) of CO gas in this system, the SnO$_2$ coatings exhibited sensor response at 25 °C when TOA addition higher than 1.00 mol%.

Fig. 9 (**a**) Resistance and (**b**) sensor response of SnO$_2$ powder coatings using various TOA addition as a function of CO concentrations at 50 °C

References

1. G.F. Fine, L.M. Cavanagh, A. Afonja, R. Binions, Sensors **10**, 5469 (2010)
2. C.S. Moon, H.-R. Kim, G. Auchterlonie, J. Drennan, J.-H. Lee, Sensors Actuators B Chem. **131**, 556 (2008)
3. M. Hjiri, L.E. Mir, S.G. Leonardi, N. Donato, G. Neri, Nanomater. **3**, 357 (2013)
4. X. Li, R. Ramasamy, P.K. Dutta, Sensors Actuators B Chem. **143**, 308 (2009)
5. N. Izu, S. Nishizaki, T. Itoh, M. Nishibori, W. Shin, I. Matsubara, Sensors Actuators B Chem. **136**, 364 (2009)
6. G.B. Barbi, J.P. Santos, P. Serrini, P.N. Gibson, M.C. Horrillo, L. Manes, Sensors Actuators B Chem. **25**, 559 (1995)
7. B. Riviere, J.P. Viricelle, C. Pijolat, Sensors Actuators B Chem. **93**, 531 (2003)
8. A. Tischner, T. Maier, C. Stepper, A. Köck, Sensors Actuators B Chem. **134**, 796 (2008)
9. Y. Shimizu, A. Jono, T. Hyodo, M. Egashira, Sensors Actuators B Chem. **108**, 56 (2005)
10. J. Kong, N.R. Franklin, C. Zhou, M.G. Chapline, S. Peng, K. Cho, H. Dai, Science **287**, 622 (2000)
11. P.-S. Cho, K.-W. Kim, J.-H. Lee, J. Electroceram. **17**, 975 (2006)
12. A. Kolmakov, Y. Zhang, G. Cheng, M. Moskovits, Adv. Mater. **15**, 997 (2003)
13. H. Long, A. Harley-Trochimczyk, T. He, T. Pham, Z. Tang, T. Shi, A. Zettl, W. Mickelson, C. Carraro, R. Maboudian, ACS Sens. **1**, 339 (2016)
14. C. Wang, L. Yin, L. Zhang, D. Xiang, R. Gao, Sensors **10**, 2088 (2010)
15. G. Korotcenkov, Mater. Sci. Eng. B **139**, 1 (2007)
16. M. Schweizer-Berberich, J.G. Zheng, U. Weimar, W. Gopel, N. Barsan, E. Pentia, A. Tomescu, Sensors Actuators B Chem. **31**, 71 (1996)
17. A. Dieguez, A. Vila, A. Cabot, A. Romano-Rodriguez, J.R. Morante, J. Kappler, N. Barsan, U. Weimar, W. Gopel, Sensors Actuators B Chem. **68**, 94 (2000)
18. B. Kim, Y. Lu, A. Hannon, M. Meyyappan, J. Li, Sensors Actuators B Chem. **177**, 770 (2013)
19. H.B. Huo, C. Wang, F.D. Yan, H.Z. Ren, M.Y. Shen, J. Nanosci. Nanotechnol. **9**, 1 (2009)
20. R. Leghrib, R. Pavelko, A. Felten, A. Vasiliev, C. Cané, I. Gràcia, J.-J. Pireaux, E. Llobet, Sensors Actuators B Chem. **145**, 411 (2010)
21. C.-Y. Chen, K.-H. Chang, Sensors Actuators B Chem. **162**, 68 (2012)
22. C.-Y. Chen, K.-H. Chang, H.-Y. Chiang, S.-J. Shih, Sensors Actuators B Chem. **204**, 31 (2014)
23. A. Mclaren, T. Valdes-Solis, G. Li, S.C. Tsang, J. Am. Chem. Soc. **131**, 12540 (2009)
24. X. Du, S.M. George, Sensors Actuators B Chem. **135**, 152 (2008)
25. A. Chiorino, G. Ghiotti, M.C. Carotta, G. Martinelli, Sensors Actuators B Chem. **47**, 205 (1998)
26. F. Hernández-Ramírez, A. Tarancón, O. Casals, J. Arbiol, A. Romano-Rodríguez, J.R. Morante, Sensors Actuators B Chem. **121**, 3 (2007)
27. C. Li, M. Lv, J. Zuo, X. Huang, Sensors **15**, 3789 (2015)
28. V.E. Bochenkov, G.B. Sergeev, in *Metal Oxide Nanostructures and Their Applications*, ed. by A. Umar, Y.B. Hahn (American Scientific Publishers, 2011), 3, pp. 31–52.
29. A. Naik, I. Parkin, R. Binions, Chemosenors **4**, 3 (2016)
30. H. Ren, H. Huo, P. Wang, C. Wang, S. Liu, M. Shen, H. Sun, M. Ruths, Int. J. Smart Nano Mater. **5**, 257 (2014)